IOP PUBLISHING PHYSICS IN MEDICINE AND BIOLOGY

Phys. Med. Biol. **52** (2007) 1335–1348 doi:10.1088/0031-9155/52/5/009

Automatic estimation of the noise variance from the histogram of a magnetic resonance image

Jan Sijbers[1,3], Dirk Poot[1,4], Arnold J den Dekker[2] and Wouter Pintjens[2]

[1] Vision Lab, Department of Physics, University of Antwerp Universiteitsplein 1, B-2610 Wilrijk, Belgium
[2] Delft Center for Systems and Control, Delft University of Technology Mekelweg 2, 2628 CD Delft, The Netherlands

E-mail: jan.sijbers@ua.ac.be, dirk.poot@ua.ac.be, a.j.dendekker@tudelft.nl and wouter.pintjens@ua.ac.be

Received 10 October 2006, in final form 19 December 2006
Published 8 February 2007
Online at stacks.iop.org/PMB/52/1335

Abstract

Estimation of the noise variance of a magnetic resonance (MR) image is important for various post-processing tasks. In the literature, various methods for noise variance estimation from MR images are available, most of which however require user interaction and/or multiple (perfectly aligned) images. In this paper, we focus on automatic histogram-based noise variance estimation techniques. Previously described methods are reviewed and a new method based on the maximum likelihood (ML) principle is presented. Using Monte Carlo simulation experiments as well as experimental MR data sets, the noise variance estimation methods are compared in terms of the root mean squared error (RMSE). The results show that the newly proposed method is superior in terms of the RMSE.

1. Introduction

The noise variance in magnetic resonance (MR) images has always been an important parameter to account for when processing and analysing magnetic resonance imaging (MRI) data. Algorithms for noise reduction, segmentation, clustering, restoration and registration highly depend on the noise variance (Nowak 1999, Zhang *et al* 2001, Ahmed 2005, Rohde *et al* 2005). Also, many applications that employ statistical analysis techniques, such as functional MRI or voxel-based morphometry, often base their conclusions on assumptions about the underlying noise characteristics (Bosc *et al* 2003, de Pasquale *et al* 2004, Sendur *et al* 2005). Finally, knowledge of the noise variance is useful in the quality assessment of the MR imaging system itself, for example to test the noise characteristics of the receiver coil or the preamplifier (McVeigh *et al* 1985).

[3] Jan Sijbers is a postdoctoral fellow of the FWO (Fund for Scientific Research—Flanders Belgium).
[4] Dirk Poot and Wouter Pintjens are doctoral students of the IWT (Institute for Science and Technology—Flanders).

In the past, many techniques have been proposed to estimate the image noise variance. These can be subdivided into two classes:

Multiple images. In the past, noise variance estimation methods were developed based on two acquisitions of the same image. A standard procedure was developed by Sano in which the noise variance was estimated by subtracting two acquisitions of the same object and calculating the standard deviation of the resulting pixel values (Sano 1988, Murphy *et al* 1993). Multiple acquisition methods are relatively insensitive to structured noise such as ghosting, ringing and DC artefacts (Sijbers *et al* 1996, 1998). However, strict requirements are the perfect geometrical alignment of the images and temporal stationarity of the imaging process.

Single image. The image noise variance can also be estimated from a single magnitude image. A common approach is to estimate the noise variance from a large, manually selected, uniform signal region or non-signal (i.e., noise only) region (Henkelman 1985, Kaufman *et al* 1989, De Wilde *et al* 1997, Sijbers *et al* 1999, den Dekker and Sijbers 2005). Manual interaction however clearly suffers from inter and intra operator variability. An additional problem is that the size of the selected (homogeneous) regions should be sufficiently large to obtain a precise estimate of the noise variance. Moreover, background data may suffer from systematic intensity variations due to streaking or ghosting artefacts.

Often, magnitude MR images contain a large number of background data. Hence, the noise variance can as well be estimated from the background mode of the image histogram. Automatic noise variance estimation have been designed from the knowledge that this background mode can be represented by a Rayleigh distribution (Brummer *et al* 1993, Chang *et al* 2005). In this paper, these procedures are reviewed and a new method is presented.

In this paper, we describe a new method to estimate the image noise variance from the background mode of the image histogram. Our initial motivation to search for a new method was that existing methods that exploit this background mode for the same purpose seemed to be based on heuristic arguments, leaving significant space for finding an improved method.

In section 2.1, the paper starts by reviewing the statistics of background MR data. Next, in section 2.2, we will describe previously reported procedures to estimate the noise variance from the background mode of the image histogram. Then, in section 2.3, we will present a new noise variance estimation method based on maximum likelihood (ML) estimation from a partial histogram. Subsequently, in sections 3 and 4, the performance of the described noise variance estimation procedures in terms of precision and accuracy are evaluated and discussed, respectively, for simulated as well as experimental data sets. Finally, in section 5, conclusions are drawn.

2. Methods

2.1. Noise properties of MR data

In MRI, the acquired complex data in k-space are known to be polluted by white noise, which is characterized by a Gaussian probability density function (PDF). After inverse Fourier transformation, the real and imaginary data are still corrupted with Gaussian distributed, white noise because of the linearity and orthogonality of the Fourier transform. However, it is common practice to transform the complex valued images into magnitude and phase images. Since computation of a magnitude (or phase) image is a nonlinear operation, the PDF of the data under concern changes. It is well known that the data in a magnitude image are no longer Gaussian but Rician distributed (Henkelman 1985, Gudbjartsson and Patz 1995):

$$p(m|A,\sigma) = \frac{m}{\sigma^2}\, \mathrm{e}^{-\frac{m^2+A^2}{2\sigma^2}}\, I_0\left(\frac{Am}{\sigma^2}\right)\epsilon(m), \tag{1}$$

with I_0 denoting the zeroth order modified Bessel function of the first kind, A the noiseless signal level, σ^2 the noise variance and m the MR magnitude variable. The unit step Heaviside function $\epsilon(\cdot)$ is used to indicate that the expression for the PDF of m is valid for non-negative values of m only.

The asymptotic approximation of the νth order modified Bessel function if its argument approaches zero is given by

$$I_\nu(z) \to \left(\frac{z}{2}\right)^\nu \Gamma(\nu+1) \qquad \text{for} \quad z \to 0. \tag{2}$$

with Γ denoting the gamma function. With (2), it is easy to show that, when the signal-to-noise ratio, defined as A/σ, is zero, the Rice PDF, given in (1), leads to the Rayleigh PDF:

$$p(m|\sigma) = \frac{m}{\sigma^2} \mathrm{e}^{-\frac{m^2}{2\sigma^2}} \epsilon(m). \tag{3}$$

The Rayleigh PDF characterizes the random intensity distribution of non-signal background areas. Its moments are given by

$$\mathbb{E}[m^\nu] = (2\sigma^2)^{\nu/2} \Gamma\left(1+\frac{\nu}{2}\right), \tag{4}$$

where $\mathbb{E}[\cdot]$ denotes the expectation operator. The first and second moments of the Rayleigh distribution are often exploited to estimate the variance of background MR data (Henkelman 1985, Kaufman *et al* 1989, McGibney and Smith 1993).

2.2. *Previously reported, histogram-based noise variance estimation methods*

Magnitude MR images generally contain a large number of background data points. Hence, the histogram of such images often shows a background mode that is clearly distinguishable from the signal contributions in the histogram. As an example, in figure 1, three coronal spin-echo MR images of a mouse brain are shown along with the corresponding histogram. The images, of size 256×256, were acquired on a 7 tesla SMIS MR imaging system, using a field of view of 30 mm in both directions. Figure 1(a) shows a proton density weighted image (TE = 20 ms, TR = 3000 ms), figure 1(c) a T_2 weighted image (TE = 60 ms, TR = 3000 ms) and figure 1(e) a T_1 weighted image (TE = 20 ms, TR = 300 ms). As can be observed from figures 1(b), (d) and (f), a background mode can easily be observed.

To estimate the noise variance from the image histogram background mode, automatic and robust noise variance estimation methods have been reported that exploit this background mode along with the knowledge that the noise-only contribution represents a Rayleigh distribution (van Kempen and van Vliet 1999, Brummer *et al* 1993, Chang *et al* 2005). In this section, these methods are reviewed. Next, in subsection 2.3, a new method is described based on ML estimation.

2.2.1. Maximum of the background mode of the histogram. From the Rayleigh PDF, given in (3), the noise variance can be estimated by searching for the value of m for which the Rayleigh PDF attains a maximum (van Kempen and van Vliet 1999):

$$\frac{\partial p}{\partial m} = 0 \qquad \Leftrightarrow \qquad 1 - \frac{m^2}{\sigma^2} = 0. \tag{5}$$

From this, it is clear that an estimate of the noise standard deviation is simply given by

$$\widehat{\sigma} = m_{\max}. \tag{6}$$

In practice, $m_{\max}$ can easily be found by searching for the magnitude value at which the background mode in the histogram attains a maximum. Since the background mode is always located on the left side of the histogram, finding this maximum is trivial.

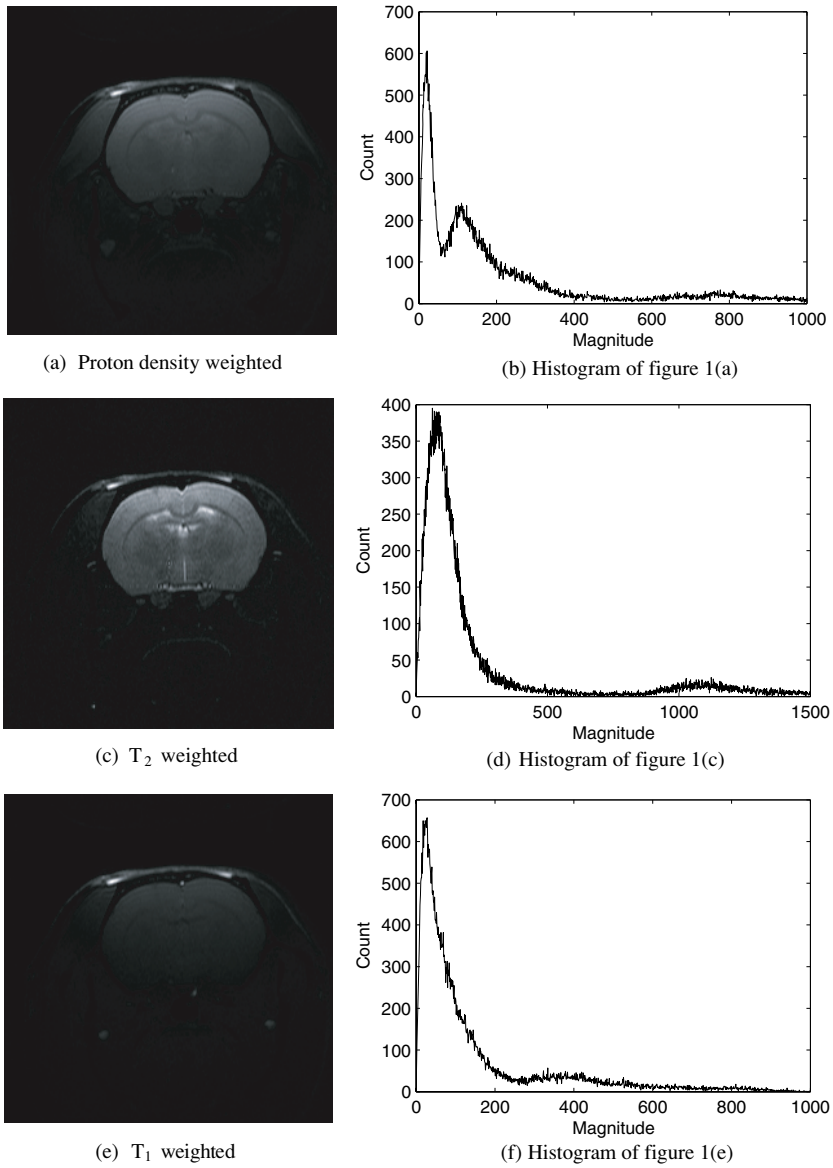

(a) Proton density weighted

(b) Histogram of figure 1(a)

(c) T_2 weighted

(d) Histogram of figure 1(c)

(e) T_1 weighted

(f) Histogram of figure 1(e)

Figure 1. 2D coronal MR image and corresponding histogram of a mouse brain: (a), (b) proton density, (c), (d) T_2, (e), (f) T_1 weighted images.

2.2.2. Brummer. In the work of Brummer *et al*, a noise variance estimation method is presented in which the Rayleigh distribution is fitted to a partial histogram using least-squares estimation (Brummer *et al* 1993):

$$\widehat{K}, \widehat{\sigma}_{\mathrm{Br}} = \arg\max_{K,\sigma} \sum_{f=0}^{f_c} \left(h(f) - K \frac{f}{\sigma^2} \mathrm{e}^{-(f^2/2\sigma^2)} \right)^2 \tag{7}$$

where K is the amplitude and σ the width of the Rayleigh distribution that is fitted to the histogram h. The cutoff f_c is defined as

$$f_c = 2\sigma_{\mathrm{Br},0}, \tag{8}$$

where $\sigma_{\mathrm{Br},0}$ is an initial estimate of the noise level. Brummer's method specifies that the position of the first local maximum of the low-pass-filtered grey-value histogram is to be used as the initial estimate. In our implementation of Brummer's method, we used Chang's estimate (see subsection 2.2.3) as an initial value.

2.2.3. Chang. In order to improve the robustness of the noise variance estimation method described in subsections 2.2.1 and 2.2.2, Chang *et al* proposed a procedure to smooth the histogram prior to estimation (Chang *et al* 2005). Thereby, a Gaussian smoothing kernel,

$$\kappa(y) = \frac{1}{\sqrt{2\pi}} \mathrm{e}^{-y^2/2}, \tag{9}$$

was used. The smoothing width h was set to

$$h = 1.06\sigma_0 n^{1/5} \tag{10}$$

in which σ_0 is the sample standard deviation and n the sample size. The smoothed histogram at signal level x is given by

$$\widehat{f}(x) = \frac{1}{nh} \sum_{i=1}^{n} \kappa\left(\frac{x - x_i}{h}\right), \tag{11}$$

where $\{x_i\}$ is the image intensity data. This smoothed histogram is then searched for the location of the first local maximum:

$$\widehat{\sigma}_{\mathrm{Ch}} = \arg\max_{\sigma} \frac{1}{nh} \sum_{i=1}^{n} \kappa\left(\frac{\sigma - x_i}{h}\right). \tag{12}$$

2.3. New noise variance estimation method

In this subsection, a new noise variance estimation method will be described based on ML estimation.

Let $\{l_i\}$ with $i = 0, \ldots, K$ denote the set of boundaries of histogram bins. Furthermore, let n_i represent the number of observations (counts) within the bin $[l_{i-1}, l_i]$, which are multinomially distributed. Then, the joint PDF of the histogram data is given by (Mood *et al* 1974)

$$p(\{n_i\}|\sigma, \{l_i\}) = \frac{N_K!}{\prod_{i=1}^{K} n_i!} \prod_{i=1}^{K} p_i^{n_i}(\sigma), \tag{13}$$

with $N_K = \sum_{i=1}^{K} n_i$ the total number of observations within the partial histogram and p_i the probability that an observation assumes a value in the range $[l_{i-1}, l_i]$. For Rayleigh distributed observations, this probability is given by

$$p_i(\sigma) = \frac{\int_{l_{i-1}}^{l_i} \frac{m}{\sigma^2} \exp\left(-\frac{m^2}{2\sigma^2}\right) \mathrm{d}m}{\sum_{i=1}^{K} \int_{l_{i-1}}^{l_i} \frac{m}{\sigma^2} \exp\left(-\frac{m^2}{2\sigma^2}\right) \mathrm{d}m}. \tag{14}$$

Since

$$\int_a^b \frac{m}{\sigma^2} \exp\left(-\frac{m^2}{2\sigma^2}\right) \mathrm{d}m = \mathrm{e}^{-\frac{a^2}{2\sigma^2}} - \mathrm{e}^{-\frac{b^2}{2\sigma^2}}, \tag{15}$$

it is easy to show that (14) simplifies to

$$p_i(\sigma) = \left(\mathrm{e}^{-\frac{l_{i-1}^2}{2\sigma^2}} - \mathrm{e}^{-\frac{l_i^2}{2\sigma^2}}\right)\left(\mathrm{e}^{-\frac{l_0^2}{2\sigma^2}} - \mathrm{e}^{-\frac{l_K^2}{2\sigma^2}}\right)^{-1}. \tag{16}$$

If the set of observations $\{n_i\}$ is fixed and σ is regarded as a variable, the joint PDF given in (13) is called a likelihood function. The ML estimate is then found by maximizing this likelihood function L with respect to σ:

$$\widehat{\sigma}_{\mathrm{ML},K} = \arg\max_{\sigma} L(\sigma|\{n_i\}, \{l_i\}). \tag{17}$$

Equivalently, the ML estimate of σ is found by minimizing $-\ln L$ with respect to σ:

$$\widehat{\sigma}_{\mathrm{ML},K} = \arg\min_{\sigma} \left[N_K \ln\left(\mathrm{e}^{-\frac{l_0^2}{2\sigma^2}} - \mathrm{e}^{-\frac{l_K^2}{2\sigma^2}}\right) - \sum_{i=1}^{K} n_i \ln\left(\mathrm{e}^{-\frac{l_{i-1}^2}{2\sigma^2}} - \mathrm{e}^{-\frac{l_i^2}{2\sigma^2}}\right)\right]. \tag{18}$$

Equation (18) is the ML estimate of the noise standard deviation from K bins. This result can be interpreted as follows. The joint PDF (13) with the ML estimate (18) as parameter generates the set of observations (counts) from which this parameter is estimated with a larger probability than a joint PDF with any other value of σ.

2.3.1. Selection of the number of bins. Note that finding the ML estimate (18) comes down to fitting a (discretized) Rayleigh PDF to the partial (left side of the) image histogram, where the criterion of goodness of fit is given by the likelihood function. This raises the question how to select the number of bins K that constitute this part. Generally, a more precise estimate (i.e., a smaller variance) will be obtained if the number of bins taken into account increases, provided that the counts in those bins are indeed Rayleigh distributed background noise contributions. However, incorporating bins with counts that can not be attributed solely to noise but also to signal contributions will introduce a bias. Hence, as a selection criterion for K, a combined measure of the bias and variance of the estimator $\widehat{\sigma}_{\mathrm{ML},K}$ was chosen. This criterion is derived as follows.

Variance. A measure of the variance of $\widehat{\sigma}_{\mathrm{ML},K}$ was constructed from the Cramér–Rao lower bound (CRLB), which is a lower bound on the variance of any unbiased estimator $\widehat{\sigma}$ of σ (van den Bos 1982),

$$\mathbb{E}[(\sigma - \widehat{\sigma})^2] \geqslant \mathbf{I}^{-1}(\sigma), \tag{19}$$

with

$$\mathbf{I}(\sigma) = -\mathbb{E}\left[\frac{\partial^2}{\partial\sigma^2} \ln p(\{n_i\}|\sigma)\right] \tag{20}$$

the Fisher information, also known as the *expected* Fisher information. It is known that the ML estimator is consistent and asymptotically most precise (i.e., it attains the CRLB asymptotically). A useful measure of the variance of $\widehat{\sigma}_{\mathrm{ML},K}$ is given by

$$\widehat{\mathrm{Var}}(\widehat{\sigma}_{\mathrm{ML},K}) = -\left(\frac{\partial^2}{\partial\sigma^2} \ln L(\sigma|\{n_i\})\Big|_{\sigma=\hat{\sigma}_{\mathrm{ML},K}}\right)^{-1}, \tag{21}$$

where the term on the right-hand side is known as the inverse of the *observed* Fisher information. This estimate of the variance was observed to be reliable only when a sufficient number of bins was taken into account. In our implementation, this number was chosen such that at least the maximum of the histogram was included.

Bias. A measure of the bias was found by quantifying the difference between the Rayleigh distribution fitted using the first K bins of the histogram and the actual bin counts in the histogram.

The histogram bin counts n_i are multinomially distributed. Furthermore, the marginal distribution of the number of counts in each bin is a binomial distribution with parameters N_K and p_i. This means that the expected value of n_i is $p_i N_K$ and its variance is $p_i(1-p_i)N_K$. However, since in general N_K is large (and p_i is small), the binomial distribution can be approximated by a normal distribution with expectation value and variance both equal to $p_i N_K$. Under the null hypothesis (H_0) that the observations in all bins are Rayleigh distributed, p_i is given by (14). Next, consider the test statistic

$$\lambda_K = \sum_{i=1}^{N} \frac{(f_{i,K} - n_i)^2}{f_{i,K}}, \tag{22}$$

with N the number of bins in the histogram and

$$f_{i,K} = p_i(\widehat{\sigma}_{\mathrm{ML},K})N_K. \tag{23}$$

It can be shown that, under H_0, λ_K is approximately χ^2_{N-2} distributed (i.e., chi-squared distributed with $N-2$ degrees of freedom). Obviously, H_0 is more likely to be rejected with increasing λ_K. Note that a large value of λ_K may indicate the presence of a bias in our estimate of σ. Therefore, λ_K will be used as a bias measure.

Most of the major contributions to λ_K can be expected to come from bins for which $i > K$, since these bins have not been taken into account in the estimation of σ. It is reasonable to assume that for these bins the counts due to the underlying, noiseless signal outnumber those due to the background noise only. Since contributions from the underlying signal can only increase the bin counts n_i, the actual bin counts will likely be significantly higher than the counts predicted by the fitted Rayleigh distribution. If we exclude the bins i with $i > K$ for which $n_i > f_{i,K}$ from (22), we obtain the modified test statistic:

$$\lambda^*_K = \sum_{i=1}^{K} \frac{(f_{i,K} - n_i)^2}{f_{i,K}} + \sum_{i=K+1}^{N} \frac{[\max(0,\, f_{i,K} - n_i)]^2}{f_{i,K}}. \tag{24}$$

The first term of (24) is known as Pearson's test statistic (Kendall and Stuart 1967), which is approximately (that is, asymptotically) χ^2 distributed with $K-2$ degrees of freedom under H_0. The second term of (24) is χ^2_M distributed under H_0, with

$$M = \sum_{i=K+1}^{N} \epsilon(f_{i,K} - n_i). \tag{25}$$

Since both terms are independent, λ^*_K is approximately χ^2_{K-2+M} distributed under H_0. Hence, the statistic

$$\widehat{b} = \frac{\lambda^*_K - (K-2+M)}{\sqrt{K-2+M}} \tag{26}$$

has approximately a standard normal distribution under H_0. The statistic (26) will be used as a measure of the bias.

Selection criterion. Finally, both measures of bias and variance given in (21) and (26), respectively, are combined into a single criterion that selects the optimal number of bins $\hat{K}$:

$$\widehat{K} = \arg\min_K [\widehat{b} + \widehat{\mathrm{Var}}(\widehat{\sigma}_{\mathrm{ML},K})]. \tag{27}$$

3. Experiments

Experiments were designed to compare the performance of the noise variance estimators discussed in subsection 2.2 to that of the newly proposed method presented in subsection 2.3. The experiments used simulated as well as experimental data. As a performance measure, the root mean squared error (RMSE) was used.

Simulated noise-only images. First, the performance of the estimators was compared using simulated, integer valued Rayleigh distributed data (corresponding to noise-only magnitude MR images), with different noise levels σ. The size of the image was 181×80.

Simulated three-modal image. Next, an image was generated that would generate one background mode and two signal modes in the image histogram. In this way, the overlap of the background mode with a signal mode could be studied. A three-modal image was obtained from an image with signal levels 0 (background), 100 and 200. Each level had an equal number of data points. Based on these levels, Rician distributed data were generated. Depending on σ, the modes overlapped which challenged estimation of the noise variance from the background mode. The size of the image was 181×240.

Simulated 2D MR image. In a next experiment, a single slice of a noise-free MR image was simulated using a web-based MR simulator (Cocosco *et al* 1997). Thereby, the normal brain database was employed (Modality: T_1 weighted; slice thickness: 3 mm; noise: 0%; intensity non-uniformity (RF): 20%). Rician distributed data with varying σ were then generated from the noiseless image obtained from the simulator. The dimensions of the slice used were 181×217.

Simulated 3D MR image. Next, a similar simulation experiment was set up as described above (i.e., using the web-based MR simulator (Cocosco *et al* 1997)), but now with a 3D MR image of size $181 \times 217 \times 60$.

Simulated 3D MR image with ghost. Furthermore, the robustness of the noise variance estimators in the presence of a ghost artefact was tested. The ghost was generated by circularly shifting the original image in one direction over half the image size in that direction and scaling the intensities to 5% of the original intensities. This ghost was then added to the original image. Also for this simulation experiment, Rician distributed noise with different σ was added.

Experimental 3D MR images. Finally, in order to test the different estimators on experimental data, a cherry tomato was scanned with a 7 tesla (Bruker, DE) MR imaging system with self-shielded gradients of 300 mT m^{-1} and an aperture of 10 cm.

To evaluate the standard deviation of the estimators experimentally, the estimators were applied to averaged images. Each averaged image was obtained by averaging over a number of images acquired under identical experimental conditions. Averaging was done in the complex *k*-space, so before reconstructing the magnitude image. The theoretical reduction of the noise standard deviation as a function of the number of images n over which the average was taken is known to be $1/\sqrt{n}$. Therefore, the estimated noise standard deviation, multiplied by $\sqrt{n}$ is expected to be constant as a function of n. In this experiment, it was tested whether the slope of the line obtained by linear regression differed significantly from zero.

4. Results and discussion

Simulated noise-only images. In figure 2, the bias and RMSE of the different estimators are shown as a function of σ. At low noise levels, Chang's estimator and the maximum estimator show an oscillatory behaviour, which is caused by the discreteness of the histogram. Indeed, at

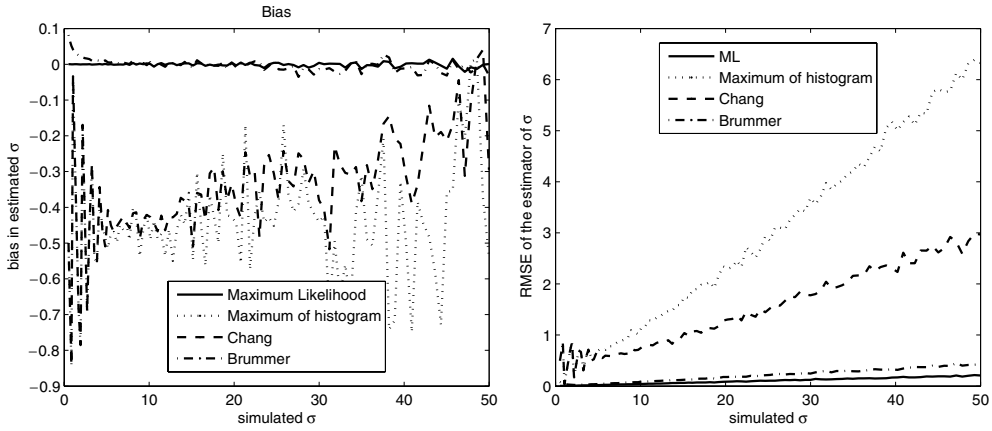

(a) Bias (b) RMSE

Figure 2. The bias (a) and RMSE (b) of the noise variance estimators as a function of σ for *simulated noise-only MR data*. For each value of σ, 2000 simulations were used.

low values of σ, the width of the Rayleigh distribution is smaller than the histogram bin width, which leads to an estimate of σ that is consistently located in the centre of the bin, which in turn has a consistent negative or positive bias. Since for low σ, the smoothing parameter of Chang's estimator given by equation (10) is too small to compensate for this effect, the oscillatory behaviour of this estimator is still apparent. For all values of σ, the maximum estimator and Chang's estimator have significantly larger RMSE than Brummer's estimator and the ML-based estimator.

Brummer's method and the ML-based method account for the Rayleigh distribution, which leads to significantly improved RMSE values of the noise variance estimator. The proposed ML-based noise variance estimator clearly performs best in terms of the RMSE because:

(i) The ML-based estimator correctly accounts for the discreteness of the data. This is especially important when σ is close to the histogram bin width. For all values of σ, only for the ML-based estimator the bias could not be shown to be significantly different from zero (which can also be appreciated from figure 2(a)).

(ii) The multinomial distribution of the histogram bins is only taken into account by the ML-based estimator. This results in a lower variance of the ML-based estimator compared to that of Brummer's estimator for a given number of bins.

(iii) The number of bins to be used for estimation is adaptively determined. For noise only data, the ML-based estimator takes generally all bins into account since they pass the Rayleigh distribution test (cf equation (24)) and thus has the lowest RMSE when the noise level is larger. In contrast, in Brummer's method, the number of bins used for estimation is determined in a 'hard' way from an initial estimate of σ (cf equation (8)).

The RMSE of the ML-based estimator is approximately half of the RMSE of the second best, which is Brummer's estimator.

Simulated three-modal image. In figure 3, the RMSE of the different estimators is plotted. As can be seen, the RMSE is low for most estimators when the signal level is below $1/3$ of the first signal level and rises sharply after that. For large σ (i.e., approximately $\sigma > 30$) the noise variance estimators yield less reliable results, because the background mode largely overlaps with the signal modes.

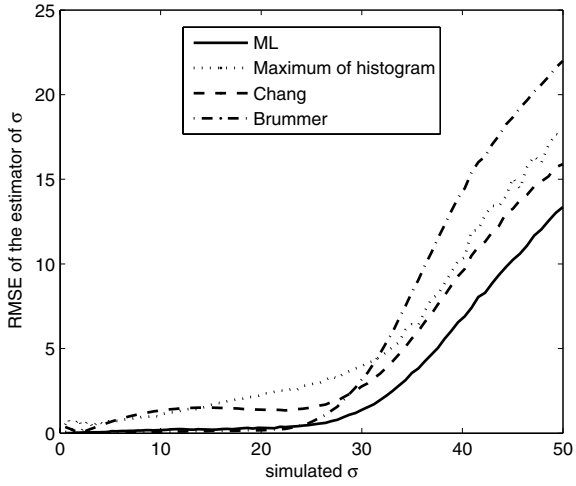

Figure 3. The RMSE of the noise variance estimators as a function of σ for a *simulated three-modal MR image*. The simulated image contained three grey values: 0, 100 and 200. For each value of σ, 500 simulations were used.

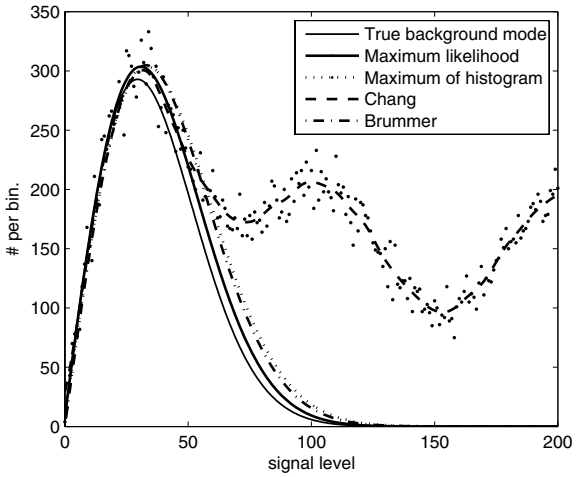

Figure 4. Histogram of the *three-modal-image* with standard deviation $\sigma = 30$, along with the true Rayleigh distribution as well as the Rayleigh distributions based on the estimated noise standard deviations and the low pass filtered histogram as specified by Chang's method.

To illustrate the difficulty of estimating σ accurately, a representative realization of the histogram with a noise level of 30 is plotted in figure 4. Along with the histogram, the true, underlying Rayleigh distribution as well as the fitted Rayleigh distributions of the different estimators are shown. As can be observed, the fitted distribution using the proposed ML-based estimation procedure approximates the true distribution best. From figure 3, it is clear that for low σ (i.e., approximately $\sigma < 30$), both Brummer's method and the ML-based method have significantly lower RMSE than the maximum estimator and Chang's estimator, which is due to the fact that much more data from the histogram are taken into account, leading to a reduced variance of the noise variance estimator. For large σ (i.e., approximately $\sigma > 30$),

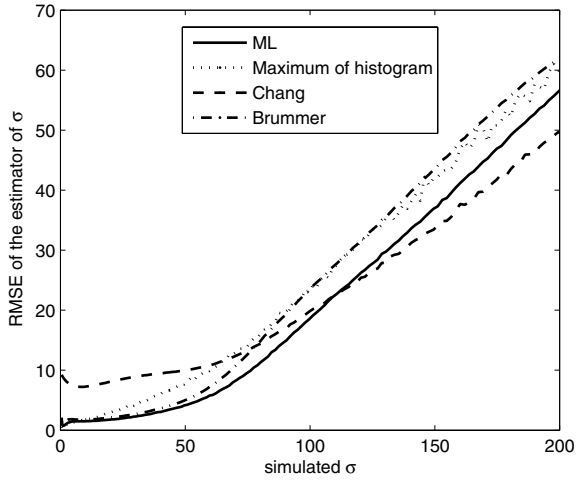

Figure 5. The RMSE of the noise variance estimators as a function of σ for *simulated 2D MR data*. For each value of σ, 1000 simulations were used.

the ML-based estimator outperforms all other estimators with respect to the RMSE. This is because the ML-based method tries to find the right balance between the variance and the bias of the σ estimator by optimizing the number of bins used for estimation.

Simulated 2D MR image. The noise variance estimation results for a simulated 2D MR image are shown in figure 5. Given the mean value $\langle m \rangle$ of the noiseless image (in this case $\langle m \rangle = 210$), the image SNR can be defined as $\langle m \rangle / \sigma$. For low SNR, Chang's method performs best, probably caused by the smoothing of the histogram. For extremely low SNR, however, none of the methods are suitable for accurate noise variance determination because in this region the signal and noise contributions in the image histogram severely overlap. For moderate or high values of the SNR (i.e., SNR > 2), the proposed ML-based noise variance estimator performs best in terms of the RMSE.

Simulated 3D MR image. The results of the simulated 3D data set are shown in figure 6(a). For 3D data sets, the ratio of the number of background voxels to the number of non-background voxels is generally significantly larger compared to 2D data sets, which facilitates the estimation of the noise variance from the histogram background mode.

In contrast to the noise-only data, Brummer's method scores worse for simulated 3D MR data than the Maximum and Chang's estimators. The main reason for this is that Brummer's estimator uses two times the initial noise σ estimate as the number of bins (cf equation (8)). When a lot of (background) data are present, as in a 3D image, the bias of this estimator becomes prominent. The ML-based method, which searches for a compromise between precision and accuracy, uses fewer bins to obtain a lower RMSE value.

Simulated 3D MR image with ghost. In figure 6(b) the results of the 3D image with ghost are presented. The change in the histogram of the noise-free image which resulted from adding the ghost is mainly concentrated in the range 10–70. The ghost seems to slightly affect the noise variance estimation for all noise variance estimation methods. However, also in this case, the proposed ML-based estimator performs best in terms of the RMSE.

Experimental 3D MR images. Finally, the noise variance was estimated from MR images of a cherry tomato. Figures 7(a) and (b) show the MR reconstruction obtained by averaging over

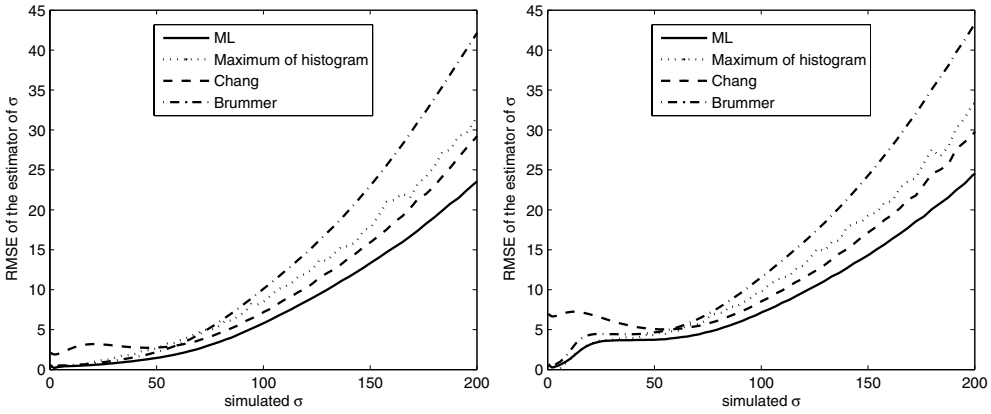

(a) No Ghost (b) with Ghost

Figure 6. The RMSE of the noise variance estimators as a function of σ for *simulated 3D-MR data*. The left image shows the results without ghost and the right image shows the results with a ghost added. For each value of σ, 500 simulations were used.

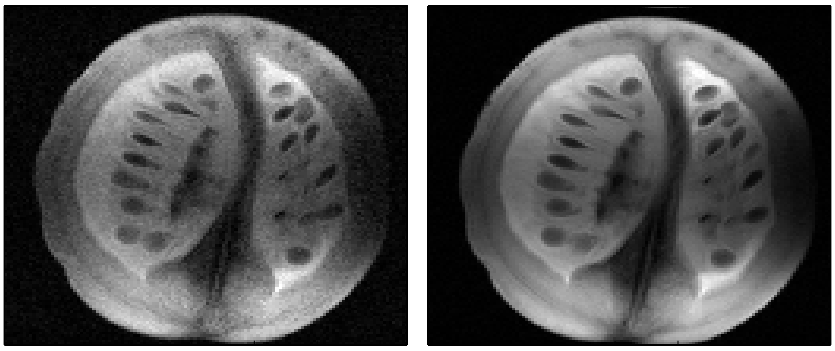

(a) No averaging (b) Average of 12

Figure 7. MR image of a cherry tomato acquired with 1 and 12 images shown in (a) and (b), respectively.

1 and 12 acquired images, respectively. The resulting $\widehat{\sigma}$ as a function of n, for each estimator, is shown in figure 8. Chang's estimator did reveal a statistically significant trend, while the other estimators did not. Note that the variance of the maximum estimator and Chang's estimator are larger than the variance of the ML-based estimator and Brummer's estimator. This is because the latter estimators exploit a larger part of the Rayleigh distributed histogram background mode.

In general, we may conclude that the RMSE of the maximum estimator performs worst of all described estimators in terms of the RMSE, mainly because the variance of this estimator is large. The RMSE of Chang's estimator is smaller than that of the maximum estimator. However, in general, its RMSE is still significantly larger than that of Brummer's and the proposed ML-based estimator. The large RMSE of the maximum and Chang's estimators can partially be explained by the fact that they do not exploit the fact that the Rayleigh distribution characterizes the background histogram bins.

Brummer's method as well as the proposed ML-based estimator do account for the Rayleigh distribution for the estimation of the noise variance. However, in general, the

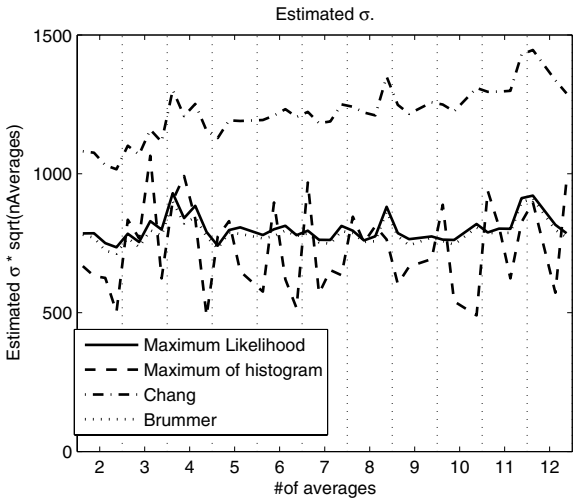

Figure 8. Estimated σ of an experimental MR image of a cherry tomato, as a function of the number of averages n used during the acquisition.

proposed ML estimator performs significantly better than Brummer's method, mainly because it selects the number of bins used to estimate the noise variance in a more optimal way.

5. Conclusions

In this paper, previously proposed noise variance estimation methods that employ the image histogram were reviewed and a new method was proposed based on maximum likelihood (ML) estimation. Simulation experiments showed that the ML-based estimator outperforms the previously proposed estimators in terms of the root mean squared error.

Acknowledgments

The authors thank Dr Robert Bos from Delft University of Technology (The Netherlands) for useful discussions.

References

Ahmed O A 2005 New denoising scheme for magnetic resonance spectroscopy signals *IEEE Trans. Med. Imaging* **24** 809–16

Bosc M *et al* 2003 Automatic change detection in multimodal serial MRI: application to multiple sclerosis lesion evolution *Neuroimage* **20** 643–56

Brummer M E *et al* 1993 Automatic detection of brain contours in MRI data sets *IEEE Trans. Med. Imaging* **12** 153–68

Chang L-C *et al* 2005 An automatic method for estimating noise-induced signal variance in magnitude-reconstructed magnetic resonance images *SPIE Medical Imaging 2005: Image Processing* vol 5747 pp 1136–42

Cocosco C A *et al* 1997 Brainweb: online interface to a 3D MRI simulated brain database *Neuroimage* **5** S425 (http://www.bic.mni.mcgill.ca/brainweb/)

de Pasquale F *et al* 2004 Bayesian analysis of dynamic magnetic resonance breast images *Appl. Stat.* **53** 475–93

De Wilde J P *et al* 1997 Information in magnetic resonance images: evaluation of signal, noise and contrast *Med. Biol. Eng. Comput.* **35** 259–65

den Dekker A J and Sijbers J 2005 Estimation of signal and noise from MR data *Advanced Image Processing in Magnetic Resonance Imaging (Signal Processing and Communications* vol 27) (Boca Raton, FL: CRC Press) pp 85–143

Gudbjartsson H and Patz S 1995 The Rician distribution of noisy MRI data *Magn. Reson. Med.* **34** 910–4

Henkelman R M 1985 Measurement of signal intensities in the presence of noise in MR images *Med. Phys.* **12** 232–3

Kaufman L *et al* 1989 Measuring signal-to-noise ratios in MR imaging *Radiology* **173** 265–7

Kendall M G and Stuart A 1967 *The Advanced Theory of Statistics* 2nd edn, vol 2 (New York: Hafner)

McGibney G and Smith M R 1993 An unbiased signal-to-noise ratio measure for magnetic resonance images *Med. Phys.* **20** 1077–8

McVeigh E R *et al* 1985 Noise and filtration in magnetic resonance imaging *Med. Phys.* **12** 586–91

Mood A M *et al* 1974 *Introduction to the Theory of Statistics* 3rd edn (Tokyo: McGraw-Hill)

Murphy B W *et al* 1993 Signal-to-noise measures for magnetic resonance imagers *Magn. Reson. Imaging* **11** 425–8

Nowak R D 1999 Wavelet based Rician noise removal for magnetic resonance images *IEEE Trans. Image Process.* **10** 1408–19

Rohde G K *et al* 2005 Estimating intensity variance due to noise in registered images: applications to diffusion tensor MRI *Neuroimage* **26** 673–84

Sano R M 1988 *MRI: Acceptance Testing and Quality Control: the Role of the Clinical Medical Physicist* (Madison, WI: Medical Physics)

Sendur L *et al* 2005 Multiple hypothesis mapping of functional MRI data in orthogonal and complex wavelet domains *IEEE Trans. Med. Imaging* **53** 3413–26

Sijbers J *et al* 1996 Quantification and improvement of the signal-to-noise ratio in a magnetic resonance image acquisition procedure *Magn. Reson. Imaging* **14** 1157–63

Sijbers J *et al* 1998 Estimation of noise from magnitude MR images *Magn. Reson. Imaging* **16** 87–90

Sijbers J *et al* 1999 Parameter estimation from magnitude MR images *Int. J. Imaging Syst. Technol.* **10** 109–14

van den Bos A 1982 Parameter estimation *Handbook of Measurement Science* vol 1 ed P H Sydenham (Chichester: Wiley) pp 331–77

van Kempen G and van Vliet L 1999 The influence of the background estimation on the superresolution properties of non-linear image restoration algorithms *Three-Dimensional and Multidimensional Microscopy: Image Acquisition and Processing VI: Proceedings of SPIE Progress in Biomedical Optics* vol 3605 ed D Cabib, C Cogswell, J Conchello, J Lerner and T Wilson pp 179–89

Zhang Y *et al* 2001 Segmentation of brain MR images through a hidden Markov random field model and the expectation maximization algorithm *IEEE Trans. Med. Imaging* **20** 45–57